



HAL
open science

Untargeted Metabolomics Reveal Lipid Alterations upon 2-Deoxyglucose Treatment in Human HaCaT Keratinocytes

Pierre Le Pogam, Mickael Doué, Yann Le Page, Denis Habauzit, Maxim
Zhadobov, Ronan Sauleau, Yves Le Dréan, David Rondeau

► **To cite this version:**

Pierre Le Pogam, Mickael Doué, Yann Le Page, Denis Habauzit, Maxim Zhadobov, et al.. Untargeted Metabolomics Reveal Lipid Alterations upon 2-Deoxyglucose Treatment in Human HaCaT Keratinocytes. *Journal of Proteome Research*, 2018, 17 (3), pp.1146-1157. 10.1021/acs.jproteome.7b00805 . hal-01730281

HAL Id: hal-01730281

<https://univ-rennes.hal.science/hal-01730281>

Submitted on 6 Jul 2018

HAL is a multi-disciplinary open access archive for the deposit and dissemination of scientific research documents, whether they are published or not. The documents may come from teaching and research institutions in France or abroad, or from public or private research centers.

L'archive ouverte pluridisciplinaire **HAL**, est destinée au dépôt et à la diffusion de documents scientifiques de niveau recherche, publiés ou non, émanant des établissements d'enseignement et de recherche français ou étrangers, des laboratoires publics ou privés.

1 **Untargeted metabolomics reveal lipid alterations upon 2-deoxyglucose treatment in human**
2 **HaCaT keratinocytes**
3
4
5

6 Pierre Le Pogam¹, Mickael Doué¹, Yann Le Page², Denis Habauzit², Maxim Zhadobov¹, Ronan
7 Sauleau¹, Yves Le Dréan² and David Rondeau^{1,3*}
8
9

10
11
12
13 ¹ Institute of Electronics and Telecommunications of Rennes (IETR), UMR CNRS 6164,
14 University of Rennes 1, Campus de Beaulieu, 263 avenue du Général Leclerc, 35042 Rennes
15 Cedex, France.
16
17
18

19 ² Transcription, Environment and Cancer Group, Institute for Research on Environmental and
20 Occupational Health (IRSET), Inserm UMR1085, University of Rennes 1, 9 avenue du Prof.
21 Léon Bernard, 35043 Rennes Cedex, France.
22
23
24

25 ³ Département de Chimie, Université de Bretagne Occidentale, 6 avenue Victor Le Gorgeu,
26 29238 Brest, Cedex, France.
27
28
29

30 *Corresponding author:

31 David Rondeau, Institute of Electronics and Telecommunications of Rennes (IETR), UMR
32 CNRS 6164, University of Rennes 1, Campus de Beaulieu, 263 avenue du Général Leclerc,
33 35042 Rennes Cedex, France.
34
35

36 tel: +33 2 23235445, email: david.rondeau@univ-rennes1.fr
37
38
39
40
41
42
43
44
45
46
47
48
49
50
51
52
53
54
55
56
57
58
59
60

Abstract

The glucose-analogue 2-deoxyglucose (2-DG) impedes cancer progression in animal models and is currently being assessed as an anti-cancer therapy. Yet, the mode of action of this drug of high clinical significance has not been fully delineated. In an attempt to better characterize its pharmacodynamics, an integrative UPLC-Q-Exactive based joint metabolomic and lipidomic approach was undertaken to evaluate the metabolic perturbations induced by this drug in human HaCaT keratinocyte cells. R-XCMS data processing and subsequent multivariate pattern recognition, metabolites identification and pathway analyses identified 8 metabolites that were most significantly changed upon a 3 h 2-DG exposure. Most of these dysregulated features were emphasized in the course of lipidomic profiling and could be identified as ceramide and glucosylceramide derivatives, consistently with their involvement in cell death programming. Even though metabolomic analyses did not generally afford such clear-cut dysregulations, some alterations in phosphatidylcholine and phosphatidylethanolamine derivatives could be highlighted as well. Overall, these results support the adequacy of the proposed analytical workflow and might contribute to a better understanding of the mechanisms underlying the promising effects of 2-DG.

Keywords: Metabolomics, Lipidomics, 2-DG, UHPLC-MS, Ceramides, Glycosylceramides, Galactosylglycerol

INTRODUCTION

An increase of aerobic glycolysis, also known as the Warburg effect,¹ is a current hallmark of cancer, leading malignant cells to have a higher glucose consumption than normal cells. As a consequence, those cells are more vulnerable to glucose deprivation.² Thus, when challenged with glycolytic inhibitors, ATP synthesis is shut off and the cell succumbs to this treatment. Accordingly, glycolytic inhibitors are increasingly regarded as a new class of anticancer agents, likely to display broad therapeutic applications.³⁻⁵ Among them, 2-deoxyglucose (2-DG), a non-metabolizable glucose analogue, was shown to strongly inhibit cancer cell proliferation and is a promising therapeutic strategy to kill cancer cells and overcome multidrug resistance.⁶ Several studies supported the subsequent assessment of 2-DG in clinical trials. Some such examples include the evaluation of 2-DG in patients having castrate-resistant prostate cancer,⁷ glioblastoma multiforme,⁸ cerebral gliomas⁹ and various advanced solid tumors.¹⁰ However, the molecular mechanisms underlying the effects of 2-DG still remain controversial.^{11,12} The addition of 2-DG to cells results in a glucose starvation-like response, even when cells are in a glucose-rich environment.^{13,14} It was also demonstrated that 2-DG can be uptaken and converted into 2-DG6P with the absence of a hydroxyl group on C₂ precluding its subsequent catabolism by phosphoglucose isomerase, which results in its accumulation.^{15,16} This accumulation might then trigger a product inhibition of hexokinase, the enzyme responsible for the rate-limiting step of glycolysis, thereby leading to a depletion of ATP. Besides, 2-DG was reported to inhibit the biosynthesis of cell wall glycoproteins and oligosaccharides, rendering the cells osmotically fragile.^{17,18} Along with these pharmacodynamics, 2-DG also inhibits N-linked protein glycosylation, competing with mannose for addition onto N-acetylglucosamine residues.¹⁹ This generates misfolded proteins which might in turn lead to endoplasmic reticulum (ER) stress. Such stress is regarded as the main mechanism by which 2-DG induces autophagy^{20,21} and apoptosis.²² Recently, a joint microarray-based and RT-PCR approach revealed that 2-DG strongly modified the transcriptome of human primary culture of keratinocyte, with the expression of 632 coding genes being modified.²³ The use of *in vitro* cell models offers advantages over other subject or animal models, which include easier experimental variables, greater reproducibility, lower cost and thus easily interpretable results.²⁴ Indeed, metabolic profiles acquired from whole organisms are strongly affected by various parameters such as gender, age,²⁵ daily habits (diet, tobacco,²⁶ coffee consumption²⁷...) that might exert significant influences on biofluids composition.

1 To the best of our knowledge, no metabolomic approaches were dedicated to unraveling the
2 promising cytotoxicity of 2-DG. Metabolomics, *i.e* the global assessment of metabolites in a
3 biological sample, represent the ‘sharp end’ of systems biology, encompassing the up-stream
4 interactions between the genome, transcriptome, and proteome.²⁸ Metabolomic strategies were
5 implemented to a variety of human studies and pinpointed several biomarkers of various diseases
6 either to be applied to early diagnosis or to monitor responses to treatments.^{29–32} Metabolomes
7 are extremely complex systems owing to the highly different physicochemical properties of
8 metabolites. As unbiased approaches, metabolomic studies should not exclude metabolite classes
9 and might rely on analytical techniques possessing high selectivity and sensitivity.³³ In order to
10 separate the hydro soluble fraction and the hydrophobic phase, different extraction procedures
11 can be assessed. Lipids of all major classes are known to be recovered *via* chloroform/methanol
12 extraction systems.^{34–36} With the introduction of the liquid-liquid Methyl tert-Butyl Ether
13 (MTBE) extractions in lipidomics,³⁷ one can consider that the use of such systems can provide
14 similar or better recovery rates of all major classes of lipids while ensuring faster and cleaner
15 recoveries compared to previous benchmark methods.³⁸ Consequently, in our work, prior to
16 undertaking large scale metabolomic studies, different extraction schemes were compared
17 differing by the nature of both the quenching and organic solvents (either MeOH or MeOH/H₂O
18 (4/1, *v/v*) and MTBE or CHCl₃, respectively). Untargeted LC-HRMS based strategies were also
19 used since they represent the prevalent strategy to detect a wide range of chemical classes and
20 thereby grant as broad a picture of metabolism as achievable.³⁹ As for related omics,
21 metabolomic workflow generates thousands of data points among which only a tiny proportion
22 might hold meaningful elements with mechanistic or explanatory power, so that relevant
23 chemometric and statistical tools are mandatory to handle such large data sets.⁴⁰

39
40 In an attempt to assess the metabolic alterations triggered upon exposure to 2-DG, a UHPLC-
41 HRMS based untargeted metabolomic approach was designed. The main aim of this
42 investigation was to delineate the molecular mechanisms underlying the effects of 2-DG on
43 human HaCaT keratinocytes, as we previously reported on transcriptomic alterations occurring
44 upon 2-DG exposure on this cell line.²³ To get the widest possible insight, lipidomic and
45 metabolomic analyses of extracellular and endocellular extracts were undertaken, both in
46 positive and negative-ion modes. Subsequently, R-XCMS data processing, multivariate pattern
47 recognition, metabolites identification and pathway analyses were delineated in the presence and
48 absence of treatment by this drug. To the best of our knowledge, this study represents the first
49 metabolomic investigation dedicated at studying the effects of 2-DG.

EXPERIMENTAL SECTION

Chemicals, reagents and materials. LC-MS grade water, methanol (MeOH), methyl tert-butyl ether (MTBE), chloroform (CHCl₃), acetonitrile (MeCN), 2-propanol (IPA), ammonium acetate, acetic acid and 2-Deoxy-D-glucose (2-DG) were purchased from Sigma-Aldrich (St. Louis, MO, USA). Phosphate-buffered saline-based cell disruption buffer was purchased from Gibco (Life Technologies, Zug, Switzerland).

The standard mixtures used for the external calibration of the MS instrument (Calmix-positive, for the positive ionization mode, consisting of caffeine, L-methionyl-arginyl-phenylalanyl-alanine acetate and Ultramark 1621, and Calmix-negative, for the negative ionization mode, consisting of acetic acid, sodium dodecyl sulfate, taurocholic acid sodium salt hydrate, Ultramark 1621) were obtained from Thermo Fisher Scientific (Waltham, MA, USA).

1,2-dipentadecanoyl-sn-glycero-3-phosphocholine (PC(15:0/15:0)), 1-pentadecanoyl-2-hydroxy-sn-glycero-3-phosphocholine (Lyso PC(15:0)), 1,2-diheptadecanoyl-sn-glycero-3-phosphoethanolamine (PE(17:0/17:0)) and N-heptadecanoyl-D-erythro-sphingosine (Cer(d18:1/17:0)) were purchased from Coger (Paris, France), L-tryptophan-2,3,3-d₃(Trypto-d₃), indole-2,4,5,6,7-d₅-3-acetic acid (Ind-AA-d₅), 1,14-tetradecanedioic-d₂₄ acid (Tetra-A-d₂₄) from C.I.L (Cluzeau Info Labo, Sainte-Foy-La-Grande, France), and 1,2,3-triheptadecanoyl-glycerol (TG (17:0)), pentadecanoic acid (C15:0), tricosanoic acid (C23:0), heptadecanoic acid (C17:0), leucine-5,5,5-d₃(Leu-d₃), Creatine-(methyl-d₃) (Crea-d₃) and lysine-4,4,5,5-d₄ (Lys-d₄) from Sigma-Aldrich. Stock standard solutions (1 mg/L) were prepared in CHCl₃ (for lipid compounds) or in MeOH and stored at -20 °C.

Internal standard (IS) solution containing C17:0, Crea-d₃ and Lys-d₄ at 10 ng/μL, lipidomic external standard (ES) solution containing (PC (15:0/15:0), Lyso PC (15:0), PE (17:0/17:0), TG (17:0), Cer (d18:1/17:0), C15:0 and C23:0 at 0.5 ng/μL and metabolomic ES solution containing Leu-d₃, Trypto-d₃, Ind-AA-d₅ and Tetra-A-d₂₄ at 1 ng/μL were subsequently prepared in CHCl₃ (lipidomic ES) or in MeOH (metabolomic ES).

Cell culture. Human keratinocyte cell line (HaCaT) was cultured as previously described.⁴¹ To exclude any problem of senescence or drift of the cellular population, the experiments on keratinocytes were conducted at earlier passages (between 4 and 10). A strict control of cell growth for subsequent normalization of metabolic profiles according to cell number is mandatory to enable cross-sample comparisons. Protein assessment was here chosen as an indicator of cell amount.⁴² For metabolomic studies, cells (seeded at a density of 60 000 cells/cm²) were transferred to six-well plates for 2 days. Then, cells were either directly processed or treated with 2-DG dissolved in water to reach a final concentration of 20 mmol/L,

1 for 3 h²³, before quenching and metabolites extraction. This treatment was previously shown to
2 induce a deep modification of gene expression.²³ To control 2-DG efficiency, the total amount of
3 ATP was evaluated from wells treated in the same conditions using an ATP Bioluminescence
4 Assay kit (Roche, Indianapolis, IN, USA). For normalization, total protein concentration was
5 assessed in parallel using a Bio-Rad DC protein assay kit (Hercules, CA, USA), and total amount
6 of ERK protein was evaluated by western blotting using anti-ERK1 (K-23) antibody (Santa Cruz
7 Biotechnology, Dallas, Texas, USA).⁴³ Real Time PCR analyses on ER-chaperons, BIP and
8 ORP150, were performed as previously described.⁴¹ Analyses were performed in triplicate and
9 Welch's two-sample *t*-test was used to compute p values between control and treated groups.
10
11
12
13
14
15
16
17

18 **Quenching and Cell Recovery.** Cell metabolism must be deactivated through the
19 quenching of biochemical processes that might alter the metabolic profiles and yield misleading
20 results.⁴⁴ Even though the trypsination and cell scraping in a buffer solution are considered as the
21 main possible approaches to harvest adherently growing cells for metabolomic studies,³⁷ the
22 trypsination treatment step is reported to damage cell membranes with possible metabolite
23 leakages,⁴⁵ and can be thereby regarded as inadequate for metabolomics.³⁷ Six-well plates were
24 thus taken out of the 37 °C incubator and immediately placed on ice during the whole workflow
25 described below.
26
27
28
29
30
31

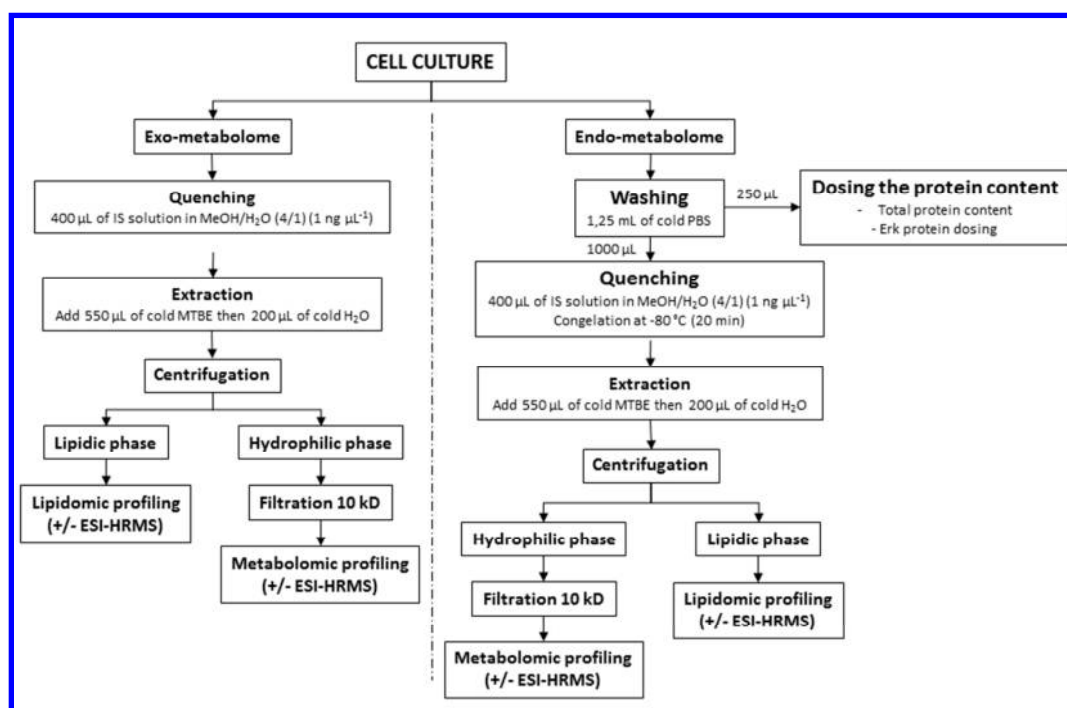
32 **Extraction procedures and Sample Preparations.** The overall metabolome comprises
33 the endo-metabolome (*i.e* metabolites present in the cells) and the exo-metabolome (*i.e*
34 metabolites encountered in the extracellular medium). As metabolites are continuously
35 exchanged between intra- and extracellular environments (owing to uptake of nutrients,
36 excretion of metabolites...), these fluxes can be monitored in the spent medium composition.⁴⁶
37 In an attempt to deepen the coverage of metabolites, the performances of several extraction
38 solvent systems were evaluated: (i) MeOH/H₂O (4/1, v/v) and MTBE, (ii) MeOH and MTBE and
39 (iii) MeOH/H₂O (4/1, v/v) and CHCl₃. As the first set of solvents afforded the best results (see in
40 Results and Discussion section), the protocol described below is established with this specific
41 system.
42
43
44
45
46
47
48
49

50 *Exo-cellular fractions.* 100 µL of the growth medium in each plate were collected into an
51 eppendorf and the rest was discarded by aspiration. To the 100 µL collected medium, 400 µL of
52 IS solution (1 ng/µL) in MeOH/H₂O (4/1, v/v) were added. The extract was further vortexed
53 (10 sec, 3 times, spaced by 1 minute break in ice) prior to adding 550 µL of MTBE. Then, 200
54 µL of cold-water were added and the same vortexing procedure was repeated. The solution was
55
56
57
58
59
60

1 further centrifuged at 12,000 g and 4 °C for 15 min. 300 μL of the upper lipidic phase were
2 transferred to a vial and 40 μL of the lipidomic ES solution (0.5 ng/μL in CHCl₃) were added
3 before evaporation to dryness under N₂ followed by reconstitution with 200 μL of
4 MeCN/IPA/H₂O (65:30:5, v/v/v) solution. For the lower hydrophilic phase (metabolomic
5 fraction), 300 μL were centrifugally filtered through a Millipore 10 KDa cutoff filter to remove
6 proteins (12 000 g, 4°C, 20 min.). 40 μL of the metabolomic ES solution (1 ng/μL in MeOH)
7 were added to the filtrated solution prior to evaporating it to dryness under N₂. The dry extract
8 was subsequently reconstituted in 200 μL of MeCN/H₂O (90:10, v/v) solution. Quality control
9 samples (QC) were prepared by mixing 20 μL aliquots of each sample. The samples were stored
10 at -80°C prior to UHPLC/MS analysis.
11
12
13
14
15
16
17
18
19
20
21
22
23
24
25
26
27
28
29
30
31
32
33
34
35
36
37
38
39
40
41
42
43
44
45
46
47
48
49
50
51
52
53
54
55
56
57
58
59
60

Endo-cellular fractions. After growth medium aspiration, the cells were washed with 1 mL of cold phosphate buffered saline solution. Cell detachment was performed by scraping cells with 1250 μL of PBS solution. A 250 μL -aliquot was recovered for subsequent dosing of the total protein content. To the remaining 1000 μL were added 400 μL of IS solution (1 $\text{ng}/\mu\text{L}$) dissolved in $\text{MeOH}/\text{H}_2\text{O}$ (4/1, v/v). In order to facilitate cell disruption and metabolite extraction, the cells were frozen at -80°C for 20 min. This solution was further added with 550 μL of MTBE and vortexed three times for 10 seconds (with one minute breaks in ice). To ensure liquid-liquid extraction, 200 μL of water were then added and the same vortexing sequence was applied. The solution was then centrifuged at 12 000 g and 4°C for 15 min. 300 μL of the upper lipidic phase were transferred to a vial and 40 μL of the lipidomic ES solution (0.5 $\text{ng}/\mu\text{L}$ in CHCl_3) were added before evaporation to dryness under N_2 followed by reconstitution with 200 μL of $\text{MeCN}/\text{IPA}/\text{H}_2\text{O}$ (65:30:5, v/v/v) solution. For the lower hydrophilic phase (metabolomic fraction), 300 μL were centrifugally filtered through a Millipore 10 kDa cutoff filter to remove proteins (12 000 g, 4°C , 20 min). 40 μL of the metabolomic ES solution (1 $\text{ng}/\mu\text{L}$ in MeOH) were added to the filtrated solution prior to evaporating it to dryness under N_2 . The dry extract was subsequently reconstituted in 200 μL of $\text{MeCN}/\text{H}_2\text{O}$ (90:10, v/v) solution. Quality control samples (QC) were prepared by pooling 20 μL aliquots of all studied samples. The samples were stored at -80°C while pending UHPLC/MS analysis.

An overview of this pipeline is provided in Figure 1.



1 **Figure 1.** Schematic workflow of the analytical process for sample preparation.
2
3
4

5 **Liquid chromatography-high resolution mass spectrometry.** Metabolomic analyses
6 were performed in a Waters Acquity UPLC chromatogram coupled online to a Thermo Q-
7 Exactive mass spectrometer. Organic phases were analyzed by the lipidomic-RPLC HRESI-MS
8 approach. Polar fractions were processed following a HILIC HRESI-MS strategy for metabolic
9 profiling purposes. In both cases, the sample injection volume was 5 μL and the flow rate was
10 set at 300 $\mu\text{L}/\text{min}$.
11
12
13
14
15

16 *Lipidomic RPLC analyses.* Reverse-phase LC separation was achieved in an Acquity
17 CSH C_{18} column (1.7 μm , 2.1 x 100 mm; Waters). Eluent solutions were
18 MeCN/ H_2O /ammonium acetate 1M/acetic acid (600/390/10/1, v/v/v/v) (solvent A) and
19 IPA/MeCN/ H_2O /ammonium acetate 1M/acetic acid (880/100/10/10/1, v/v/v/v/v) (solvent B). A
20 25 min gradient was performed as follows: the initial solvent system consisted of 60% A and
21 40% B. For the two first minutes, the gradient was linearly changed to 50% A and 50% B. Then,
22 the proportion was increased to reach 70% B at 12 minutes. The final elution conditions (1% A
23 and 99% B) were obtained at 17 min and held for 8 minutes. Afterwards, the initial conditions
24 were recovered and maintained for 4 minutes for column conditioning. Samples were ionized in
25 positive and negative-ion modes with ESI parameters as follows: sheath gas flow, 55 Arbitrary
26 Units (AU); auxiliary gas flow, 10 AU; capillary temperature, 300°C; spray voltage, 3.5 kV; S-
27 lens radiofrequency, 50 AU. HMRS data were acquired in full-scan mode over the m/z range
28 150-1500 at a resolving power of 35 000 Full Width Half Maximum (FWHM) at m/z 200. The
29 Automatic Gain Control (AGC target) was set at high dynamic range (5×10^5) with a maximum
30 injection time of 100 ms.
31
32
33
34
35
36
37
38
39
40
41

42 *Metabolomic HILIC analyses.* HILIC chromatography was performed in a SeQuant ZIC-
43 HILIC column (3.5 μm , 2.1 x 100 mm, Merck). The mobile phase consisted of H_2O /ammonium
44 acetate/acetic acid (980/10/1, v/v/v) (solvent A, adjusted at pH 4.75) and of MeCN/solvent A
45 (950/50) (solvent B). The elution sequence lasted 16 min and was programmed as follows: the
46 initial conditions (5% A; 95% B) were maintained for two minutes prior to being linearly
47 modified to 20% A and 80% B at 5 min. The proportion of phase A was linearly increased to
48 reach 40% at 12 min. The final plateau (60% A and 40% B) was obtained at 14 min and held for
49 2 min. To condition the column, the initial conditions were then recovered for 10 min. Samples
50 were ionized in positive and negative-ion modes with ESI parameters as follows: sheath gas
51 flow, 55 AU; auxiliary gas flow, 10 AU; capillary temperature, 300°C; spray voltage, 3.0 kV; S-
52
53
54
55
56
57
58
59
60

1 lens radiofrequency, 50 AU. HRMS data were acquired in full-scan mode over the m/z range 65-
2 975 at a resolving power of 35000 FWHM at m/z 200. The Automatic Gain Control (AGC
3 target) was set at high dynamic range (5×10^5) with a maximum injection time of 100 ms.
4
5
6
7

8 **Quality control.** Each sample was analyzed 6 times in a randomized batch sequence.
9 Prior to each batch analysis, the mobile phase was run for 1.5 h, followed by six QC samples to
10 enable proper column equilibration and conditioning. To monitor and overcome analytical drifts
11 in UPLC-MS, quality control samples were injected at regular intervals during the experimental
12 sequence (*i.e.* every 8 samples), in line with published guidelines.⁴⁷ For each analysis, the ions
13 that were detected during either the dead volume (<0.6 min) or the conditioning of the column
14 (>26 min) were eliminated. Features were considered reproducible if their Coefficient of
15 Variation (CV) among QC samples were below 30%, as suggested elsewhere.^{48,49} Adversely,
16 features that did not respect this condition were removed from the data subset. To further assess
17 the validity of the analytical strategy described herein and assist in retention time correction,
18 external isotope-labeled metabolites were added after the extraction process as detailed earlier.
19 These standard metabolites were selected to encompass a wide range of polarities and chemical
20 structures. Thus, their retention times span across the whole chromatogram. Internal standards
21 (*i.e.* endogenous metabolites added prior to sample extraction) were also included to track sample
22 extraction efficiency.
23
24
25
26
27
28
29
30
31
32
33

34 **Data processing.** Raw data were processed using R-XCMS to help with the putative
35 identification of potential biomarkers of exposure to 2-DG. XCMS workflow involves typical
36 data processing steps including peak discrimination, peak filtering and peak alignment. This
37 workflow generates a data matrix presented as a feature list comprising their integrated
38 intensities (Extracted Ion Chromatogram peak area) along with the corresponding Fold Change
39 (FC) and associated ANOVA p-values.⁵⁰ Final peak picking parameters were: prefilter=(c,
40 average chromatographic signal/10), peak width =c(5,25), snthresh=6, mzdif= 0.01, ppm= 15.
41 Alignment (bw = 9, minfrac= 0.66, minsamp= 4, mzwid= 0.008) and retention time correction
42 (obiwarp, plotype = c(deviation), profstep= 1). Regarding univariate analyses, the Coefficient of
43 Variation (CV) within QC samples was obtained by dividing the standard deviation by the mean
44 intensity of each feature, and a histogram displaying the CV distribution was generated. Then,
45 the computation of the Fold-Change ratio (FC, relating abundance between control and treated
46 samples) along with the corresponding ANOVA p-value (statistical significance from a Student
47 *t*-test) streamlined the selection of the features of interest. The frames of interest were selected
48 according to the following criteria: CV QC < 30%, FC > 2 and ANOVA p-value < 0.05. At this
49
50
51
52
53
54
55
56
57
58
59
60

1 stage, Extracted Ion Chromatograms were individually checked to retain as putative biomarkers
2 the features for which no overlap occurred between control and 2-DG treated samples. Box and
3 Whiskers plot related to all metabolites of potential interest were individually checked to retain
4 the features for which limited to null overlap existed between control and treated values.
5 Practically speaking, the features for which the 75th percentile of the sample group displaying the
6 lower value was below the 25th percentile of the sample group having the higher value were
7 selected as potential biomarkers of exposure. Horizontal lines appearing in the boxes illustrate
8 the median, bottom and top boundaries of boxes refer to the lower and upper quartiles, at last
9 whiskers depict the 5th and 95th percentiles. Multivariate analyses by Principal Component
10 Analysis (PCA) were performed using Progenesis QI (v. 2.1) (Non-linear Dynamics, Newcastle-
11 upon-Tyne, UK).

21 **Tentative identification of metabolites.** The tentative identification of the metabolites of
22 interest was carried out as follows. The exact masses of their monoisotopic molecular weight
23 were tentatively identified against the Progenesis Metascope “Biomolecules” database, and the
24 free online databases, including METLIN^{51,52} (<http://metlin.scripps.edu>) and HMDB^{53,54}
25 (<http://www.hmdb.ca/>). Metabolite hits were searched for with a tolerance of ± 5 ppm for both these
26 databases considering several possible monoisotopic masses for each feature of interest (protonated
27 molecules, ion adducts...). For lipidomic sequences, LipidMaps online database⁵⁵ (University of
28 California, San Diego, CA – www.lipidmaps.org) was also consulted to elect the most suitable
29 markers, considering a maximum adopted mass accuracy error of ± 5 ppm.

RESULTS AND DISCUSSION

Assessing the cellular effects of 2-DG. First of all, ATP concentration and expression levels of the mRNA of two ER-resident chaperons, BIP (immunoglobulin heavy-chain binding protein, also named HSPA5) and ORP150 (oxygen regulated protein 150 kDa, or HYOU1), were measured, following experimental procedures which some of us previously described.⁵⁶ The results depicted in Figure 2 reveal that 2-DG treatment of HaCaT keratinocyte cells leads to (i) a depletion in intracellular ATP (*i.e.* 10-fold decrease of ATP concentration, Figure 2a, $P = 0.00283$, Welch two-sample t test) and (ii) an increase of the expression of the ER-stress sensors BIP/ORP150 as the cell lines are exposed to 2-DG (see Figure 2b) ($P = 0.00286/0.00292$, respectively, Welch two-sample t -test). These results are in agreement with the literature^{57,58} and underline the effectiveness of 2-DG treatment.

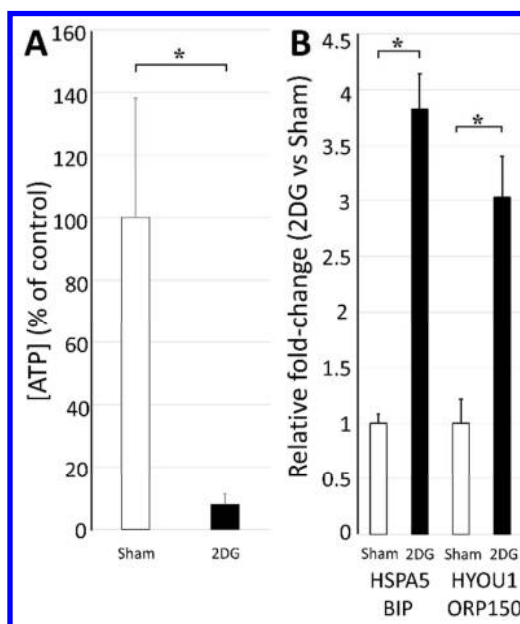


Figure 2. Comparison of intracellular ATP content (A) and mRNA levels of ER-resident chaperons involved in ER stress response (HSPA5/BIP and HYOU1/ORP150) ($n = 3$) (B) upon 2-DG treatment. * $P < 0.01$, Welch two-sample t test.

Optimization of the extraction procedure. Three extraction procedures were compared using the following experimental setups (i) MeOH/H₂O (4/1, v/v) and MTBE, (ii) MeOH and MTBE and (iii) MeOH/H₂O (4/1, v/v) and CHCl₃. These sample processing methods were attempted on three different control samples that were subsequently submitted to the previously described metabolomic workflow (*i.e.* each sample analyzed 6 times, in a randomized sequence). These different procedures were compared with respect to the number of detected features and proportions of ions with CV below 30%, with the results being collated in Table S1. Regarding the number of detected features, all three approaches granted results that were consistent there

1 between. Nevertheless, results obtained with the MeOH/MTBE approach revealed a reduced
2 proportion of features having a CV QC < 30% in lipidomic sequences. The outcomes of the
3 MeOH/H₂O/MTBE and MeOH/H₂O/CHCl₃ procedures afforded somewhat equivalent results as
4 the former provided a higher proportion of ions with CV QC < 30% in endocellular fractions and
5 *vice versa*. Considering the nearly equal performances of these approaches, the known
6 carcinogenicity of CHCl₃⁵⁹ streamlined the choice of MeOH/H₂O/MTBE for the definitive
7 experimental setup. A further drawback of chloroform over MTBE is that it might decompose
8 into phosgene and hydrochloric acid which might chemically alter labile lipid species.⁶⁰ Similar
9 mixtures of MTBE, MeOH and H₂O were already reported to simultaneously extract
10 metabolome and lipidome in a satisfying manner.⁶¹⁻⁶³ Global metabolomic and lipidomic
11 analyses afforded a comprehensive coverage of the non-polar and polar fractions of HaCaT cells,
12 respectively.

21
22
23 **Data quality assurance.** With respect to quality control assessments, the following
24 procedures were always applied prior to data acquisition and analysis: comparison of column
25 pressure to that of the previous run, assessment of the internal standard variations between QCs
26 and study samples as well as instrumental stability across the whole batch analyses (in terms of
27 reproducibility of retention times and accurate masses). These criteria guided the acceptance
28 of the analytical strategy undertaken herein. Likewise, retention drift observed throughout the
29 different sequence analyses served as a further ground for the acceptance of the analytical runs.

34
35
36 In lipidomics, the retained external standards were phosphatidylcholine (15:0) (RT 8.37
37 min), lysophosphatidylcholine (15:0) (RT 1.75 min), ceramide (d18:1) (RT 17.95 min), C15:0
38 (RT 3.19 min), C23:0 (RT 9.27 min). C17:0 (RT 4.30 min) served as an internal standard.

41
42 Metabolomic analyses included leucine-d₃ (RT 5.97 min), tryptophan-d₃ (RT 6.10 min),
43 indole acetic acid-d₅ (RT, 1.81 min), tetradecanedioic acid-d₂₄ (RT 1.38 min) as external
44 standards. Creatine-d₃ (RT 8.22 min) and L-lysine-d₄ (RT 14.31 min) were selected as internal
45 standards.

48
49
50 Peak area and intensity repeatability for the isotope-labeled standards were considered
51 with a threshold of 30% CV, following the widely admitted idea that ions displaying higher CV
52 values might not represent fitting candidates when searching for biomarkers.⁶⁴ All isotope-
53 labeled standards fulfilled these conditions, with CV among QC samples being constantly below
54 15% (Tables S2 and S3 for lipidomic and metabolomics sequences, respectively).

Likewise, data sets having greater than 70% of the ions with CV values among QC samples below 30% are considered acceptable for further data processing.^{65,66} Depending on the studied fraction, these values ranged between 71.8 and 93.9% (Table 1), consistently with metabolomics guidelines.⁶⁵

Table 1. Ion features obtained using R-XCMS data processing

Metabolome	Fraction	Ion mode	Ions	Ions with CV QC < 30% (% of total ions)	Ions (isotopes)	Ions with (fold-change > 2 and p-value < 0.05)
Exo	Lipido	Positive	4125	3710 (89.9)	2242	92
		Negative	1129	989 (87.6)	713	29
	Metabo	Positive	1838	1711 (93.1)	1379	21
		Negative	1233	1158 (93.9)	882	63
Endo	Lipido	Positive	4241	3574 (84.3)	2182	42
		Negative	1427	1024 (71.8)	710	35
	Metabo	Positive	1748	1546 (88.4)	1290	95
		Negative	1037	925 (89.2)	745	30

Both these results underscored the reliability of the analytical strategy developed herein.

Extracellular profiles were overwhelmed by the signals arising from 2-DG, failing to reveal any further difference upon exposure to this drug (data not shown). Therefore, only endocellular fraction profiles will be further considered in this manuscript.

Lipidomic RPLC-MS analyses of endocellular fractions. Data processing yielded a number of detected ions aligned by their retention time, accurate masses and peak areas. The data matrix was filtered out as previously indicated, leading to retain 710 and 2182 ions in negative and positive-ion modes, respectively. Establishing PCA loading plots represented a first pertinent step to determine if the metabolic data could successfully separate the two groups. These plots (Figure S1) revealed that control and treated groups clustered separately, whatever the considered ionization mode, indicating distinct metabolic responses between the control and 2-DG-treated groups. The discrimination between sample groups can be made clearer yet when only retaining the features having a Fold-Change (FC) > 2 with an ANOVA p-value below 0.05 (and a CV QC below 30%) (Figure S2).

Overall, 42 features in positive-mode and 35 in negative-ion mode were selected as potential biomarkers of exposure to 2-DG (*i.e.* CV among QC samples < 30%, p-value < 0.05 and fold-change > 2). The careful validation of both Extracted Ion Chromatograms and Box and Whiskers Plot (as described in the Data processing part of the Experimental section) (Figure 3)

for these putatively dysregulated features led to retain 8 candidate ions as biomarkers of exposure to 2-DG, genuinely corresponding to 6 metabolites (Figure 3, Table 2) as two of these putative biomarkers were found to occur in both positive and negative-ionization modes (M791T825/M827T825 and M819T887/M855T887 (positive-ion mode/negative-ion mode)).

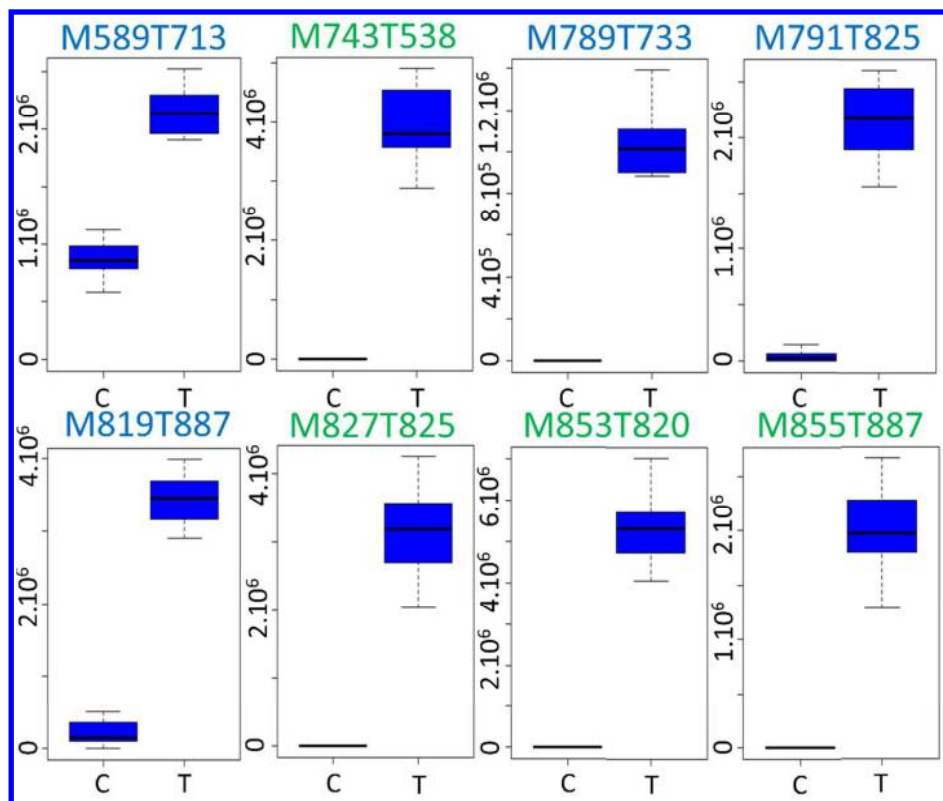


Figure 3. Box and whisker plots of the candidate biomarkers of treatment by 2-DG highlighted by lipidomic RPLC-MS analyses ($n = 6$). The y axis displays the normalized intensity of each metabolite. Features are designated as MXXXTYYY with XXX being the monoisotopic mass and YYY the retention time of the ion. Associated FC and ANOVA p-values are provided in Table 2. Features typed in blue were detected in positive-ion mode and those appearing in green arose in negative polarity.

Accurate mass measurements from these ions were primarily searched against the freely available database LipidMaps, leading to retrieve a list of potential identifications based on previously defined accurate mass error ranges. Further searches were then carried out on METLIN and HMDB to check whether further identifications could be retrieved but none of these databases led to propose other putative hits. All these dysregulated features could thus be identified as a ceramide and different glucosylceramides (Table 2). The biomarker M589T713 could be identified as a Cer(36:1), with several putative structures differing in the length and unsaturation degrees of the side chains being possible, as listed in Table 2. From a biological

viewpoint, all these long-chain ceramides display similar pro-apoptotic and anti-proliferative effects.^{67,68} Ceramides permeabilize the mitochondrial outer membrane, initiating mitochondrial-mediated apoptosis through the release of cytochrome c.⁶⁹ Besides this non-protein-mediated signal, a variety of downstream signals involving an array of specific targets also account for ceramide-mediated apoptosis or autophagy. These molecular effects were recently reviewed in the specific context of mammalian epidermidis cells.⁷⁰ Being widely encountered in nature, glucosylceramides are glycolipids bearing a hydrophilic head group sugar, D-glucose, and two hydrophobic aliphatic chains (typically 16 to 26 atoms long) that vary in both length and saturation.⁷¹ Glycosylceramide synthases are indeed known to convert ceramides into nontoxic glucosylceramides tending to offer cell protection and priming various cell types for proliferation,⁷²⁻⁷⁴ contributing to convey multi-drug resistance.^{75,76} Owing to these opposite effects, the Cer-to-GlcCer ratio appears to modulate cellular growth versus apoptosis and it was demonstrated that human HaCaT keratinocyte cells might favor ceramide to glucosylceramide conversion to overcome ceramide cytotoxic effects.⁷⁷ Among the 5 glucosylceramides identified as dysregulated in the course of this manuscript, two could be associated with a single hit, *i.e.* M791T825/M827T825 (GlcCer (d18:0/22:0)) and M819T887/M855T887 (GlcCer (d18:0/24:0)). Two glucosylceramide candidates might be responsible for the three remaining hits, preventing us from reaching an unambiguous structural assignment. Nevertheless, the current data enables determining the overall number of carbons and unsaturations of the side chains, granting a sum composition expressed as (total carbons : total double bonds), as suggested by current lipidomic guidelines.⁷⁸ As such, M743T538 could be related to the molecular formula GlcCer (36:1), M789T733 to GlcCer (40:1) and M853T820 to GlcCer (42:1). The two possible structures for these latter are provided in Table 2. Regarding the biological function of glucosylceramides, their effects were not so far evidenced to depend on the constitution of the fatty acid side chains, not even being shown to vary according to the sum composition of these structures.⁷⁹ Thus, satisfying biological conclusions can be drawn from the biochemical data garnered herein on these biomarkers. Accordingly, in the current study, glucosylceramides were much more up-regulated than the identified ceramide which displayed a moderate FC value of 2 (Table 2). The metabolomic study reported herein seems to unveil that HaCaT keratinocyte cells implement a similar defense strategy. A possible way to validate this putative scenario would be to monitor the expression of these dysregulated features following different times of treatment with 2-DG. One can indeed assume that these up-regulations might refer to a two-step process that would begin with an increase of ceramide to be subsequently counteracted by an increased production of glucosylceramides, as a cytoprotective mechanism. These lipidomic dysregulations are consistent with former studies that reported on the alteration of total levels and/or species

1 compositions of several lipid classes. Kavaliauskiene et al. (2015) also reported on an
2 upregulation of ceramide derivatives in HEP-2 cells, which is in line with the outlined results.
3 Conversely, this cellular system also responded by a slight decrease in GlcCer derivatives.⁸⁰
4 HRMS² analyses might be relevant to distinguish between candidate structures for ambiguous
5 ceramides and glucosylceramides reported herein, indicating the acyl composition of the
6 highlighted biomarkers. Nevertheless, the current knowledge on the role of each one of the lipid
7 molecular species (*i.e* taking into account the lipid group and exact constitution of the side
8 chains) are too scarce to explain their role on an individual basis. Therefore, it can be surmised
9 that assigning ceramides and glucosylceramides to a sum composition according to the shorthand
10 nomenclature defined by the International Lipid Classification and Nomenclature Committee⁸¹
11 provides enough information as to the biological relevance of these dysregulations, as often done
12 elsewhere.^{82,83}
13
14
15
16
17
18
19
20
21
22
23
24
25
26
27
28
29
30
31
32
33
34
35
36
37
38
39
40
41
42
43
44
45
46
47
48
49
50
51
52
53
54
55
56
57
58
59
60

Table 2. List of potential metabolite candidates dysregulated upon 2-DG treatment, assessed in both positive and negative lipidomic analyses. These putative identifications were obtained after a search in the LipidMaps database with a cutoff of ± 5 ppm. *HaC: acetic acid. Elemental compositions, theoretical masses and errors for these features are provided in Table S6.

RT (sec.)	Exact mass (of m/z signal)	LipidMaps hits (0.003 Da)	LipidMaps ID	Detected ion/Adduct ion	P-value	Fold-change	CV QC (%)
538.13	742.5851	GlcCer(d16:1(4E)/20:0(2OH))	LMSP0501AA76	[M-H] ⁻	1.3E-8	∞	22.7
		GlcCer(d14:1(4E)/22:0(2OH))	LMSP0501AA66				
713.41	588.5328	Cer(d14:1/22:0)	LMSP02010038	[M+Na] ⁺	2.3E-10	2.0	6.4
		Cer(d16:1/20:0)	LMSP02010047				
		Cer(d18:0/18:1)	LMSP02020015				
		Cer(d18:1/18:0)	LMSP02010006				
733.12	788.6332	GlcCer(d16:1/24:0)	LMSP0501AA51	[M-H ₂ O+Na] ⁺	3.0E-7	90.2	28.2
		GlcCer(d18:1/22:0)	LMSP0501AA07				
819.99	852.6941	GlcCer(d18:0(4E)/24:1(15Z))	LMSP0501AA22	[M-H ₂ O+HaC-H] ^{-*}	1.0E-8	∞	13.9
		GlcCer(d18:1/24:0)	LMSP0501AA09				
825.01	790.6478	GlcCer(d18:0/22:0)	LMSP0501AA21	[M-H ₂ O+Na] ⁺	3.0E-9	4.1	26.4
825.37	826.6782		[M-H ₂ O+HaC-H] ^{-*}	1.6E-7	∞	18.7	
887.13	818.6823	GlcCer(d18:0/24:0)	LMSP0501AA23	[M-H ₂ O+Na] ⁺	2.3E-13	15.3	15.5
887.43	854.7089			[M-H ₂ O+HaC-H] ^{-*}	1.7E-7	∞	0

Metabolomic HILIC-MS analyses of endocellular fractions. Irrespective of the ionization mode, PCA plots failed to reveal a clear cut separation when all m/z signals were used (Figure S3). Nevertheless, when only plotting the significantly altered m/z values upon 2 DG exposure (*i.e* p -value < 0.05 and fold-change > 2 with CV among QC samples < 30%), PCA plots resulted in a satisfying discrimination in both ion modes (Figure S4). As reported in Table 1, this filtered data set corresponded to 95 and 30 features in positive and negative-ion modes, respectively. Data processing and analysis emphasized 7 molecular features as major contributors to the variance between treated and control cells (Figure 4, Table 3). These metabolites of interest were tentatively identified against METLIN and HMDB databases which could lead to propose putative identifications for all 7 features. Among these ions, only one, M277T435/M289T441, indicated a clear-cut dysregulation between the two sample groups, as previously reported for lipidomic sequences (Figure 4). This metabolite could be tentatively identified as galactosylglycerol but the biological relevance of this dysregulation still remains to be determined. With respect to the six remaining features, multiple putative identifications could be retrieved from freely available databases. Overall, these hits could be identified as phosphatidylcholine or phosphatidylethanolamine derivatives (Tables 3 and S4). More precisely, three biomarkers M809T320/M821T328, M719T328 and M747T329 could be related to this former class of lipids. Conversely, M751T169 could be identified as a phosphatidylethanolamine derivative. Regarding the two last biomarkers highlighted throughout the lipidomic workflow, putative hits could be retrieved from both phosphatidylcholine and phosphatidylethanolamine series. Generated results were assessed by regards to their physicochemical properties. Taking into account LogP values could narrow down the identification possibilities for these metabolites leading to tentatively identified them either as a phosphatidylethanolamine or a phosphatidylcholine derivative (Table S5). As to M719T191, LogP values associated with the phosphatidylcholine candidates are not in line with the retention time obtained for this feature. Likewise, phosphatidylethanolamine candidates proposed for M761T326/M795T331 are too apolar to fit the retention time of this feature. Therefore, it can be assumed that M719T191 might stand for a phosphatidylethanolamine derivative and that M761T326/M795T331 corresponds to a further phosphatidylcholine-derived metabolite. Altogether, these data can lead to define a list of possible biomarkers related to a single structural series for all dysregulated features. Even though the lack of these substances as commercially available standards precluded the individual identification of these metabolites, each feature could be associated with a global number of carbons for the two side chains as well as an overall number of unsaturations, as earlier described for ceramide and glucosylceramide derivatives (Table 3). The close physicochemical properties and identical matrices of occurrence precluded unambiguous structural assignments among the

1 remaining candidates. Further HRMS² analyses might be relevant to further discriminate
2 between the possible candidates garnered in Table 3 even though reaching unambiguous
3 structural assignments might be very hard to achieve, owing to the multiple possible positions of
4 unsaturations, in particular. Not being able to discriminate among putative glycerophospholipids
5 displaying an identical number of carbons and unsaturations is not believed to represent a severe
6 limitation of the current work. Indeed, phosphatidylcholines represent a highly complex family
7 of 1,2-diacylglycerophospholipids, that are mainly known through their structural role as
8 essential components of cell membranes. These metabolites have in common a zwitterionic
9 structure comprising hydrophobic side chains differing in their lengths and unsaturation degrees.
10 So far, the biological role of these glycerophospholipids has been primarily defined by regards to
11 the overall chain length and not an individual molecule basis.⁸⁴ Accordingly, metabolomic
12 investigations reporting on perturbations of glycerophospholipid content often define the global
13 number of carbons and number of double bonds, as performed here.⁸⁵⁻⁸⁷ As to the dysregulated
14 phosphatidylethanolamine derivatives, it is worth noting that they display an identical number of
15 carbons and unsaturations than phosphatidylcholine derivatives emphasized herein. Therefore,
16 the former might represent biosynthetic intermediates en route to the latter.⁸⁸ Moreover, the level
17 of these phosphatidylcholine and phosphatidylethanolamine derivatives are only poorly altered
18 after 2-DG treatment with FC being always comprised between 2 and 3, so these effects might
19 not be of paramount importance to understand the effects of this cytotoxic drug, further limiting
20 the interest of reaching an unambiguous structural assignment of these features.
21
22
23
24
25
26
27
28
29
30
31
32
33
34
35
36
37
38
39
40
41
42
43
44
45
46
47
48
49
50
51
52
53
54
55
56
57
58
59
60

Table 3. List of potential metabolite candidates dysregulated upon 2-DG treatment, assessed in both positive and negative metabolomic analyses. These putative identifications were obtained after a search in the HMDB database with a cutoff of ± 5 ppm. Associated FC and ANOVA p-values are provided in Table 2. *HMDB hits indicated between brackets display inconsistent physicochemical parameters (Table S5). **Owing to the elevated number of candidates, the exact references of hits along with the associated HMDB IDs are collated in Table S4. Elemental compositions, theoretical masses and errors for these features are provided in Table S7.

RT (sec.)	Exact mass (of m/z signal)	HMDB hits	HMDB ID	Detected ion/Adduct ion	P-value	Fold- change	CV QC (%)
168.96	750.5417	PE (38:5)	**	$[M+H]^+$	0.009	2.8	25.1
		PE (36:2)	**	$[M+Na]^+$			
190.99	718.5370	PE (34:1) PC (31:1)*	**	$[M+H]^+$	0.009	2.5	27.1
320.48	808.5834	PC (36:2)	**	$[M+Na]^+$	0.006	2.1	4
327.58	820.5603			$[M+Cl]^-$	0.004	2.5	26.1
326.18	760.5840	PC (34:1)	**	$[M+H]^+$	0.004	2.1	5.7
331.13	794.5475	PE (37:1)*		$[M+Cl]^-$	0.004	2.1	9.1
328.30	718.5775	PC (32:0)	**	$[M+H]^+$	0.004	2.2	8.5
328.92	746.6057	PC (34:0)	**	$[M+H]^+$	0.002	2.5	8.6
435.15	277.0891	Galactosylglycerol	HMDB06790	$[M+Na]^+$	1.3E-8	1035	22.5
441.00	289.0700			$[M+Cl]^-$	1.7E-5	228	28.3

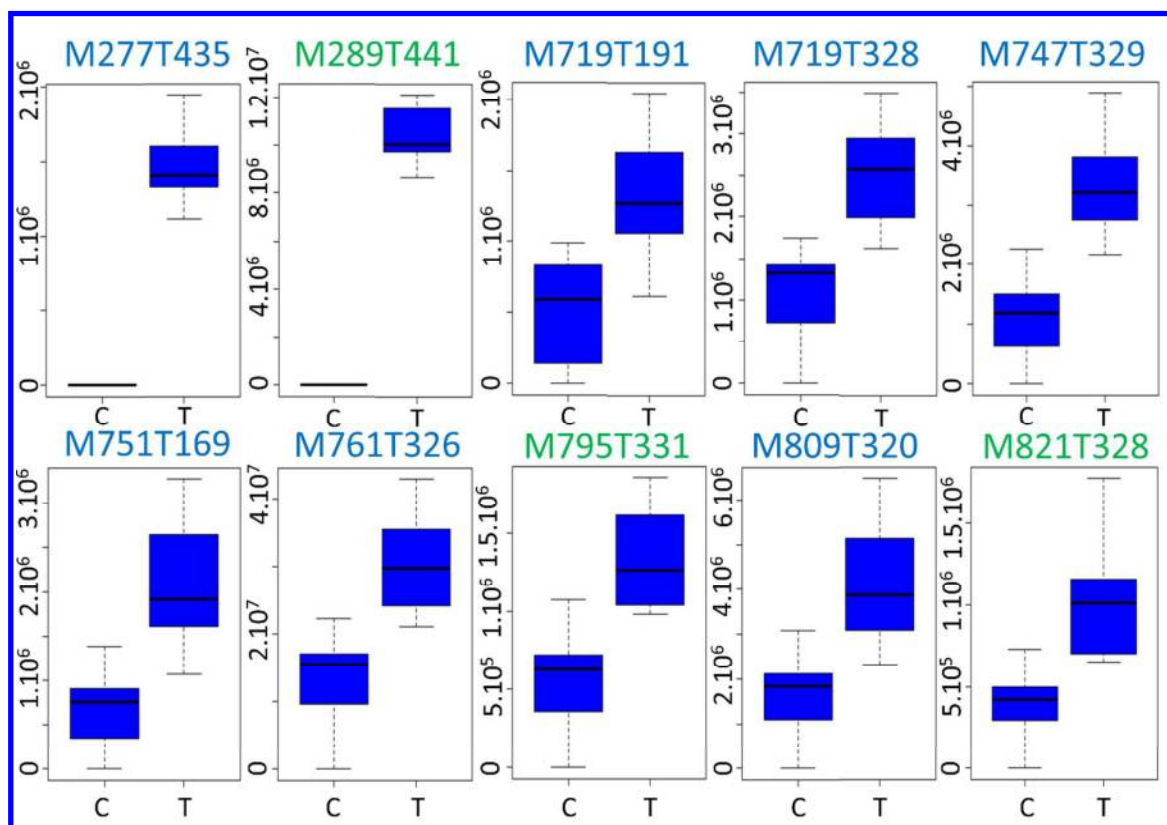


Figure 4. Box and whisker plots of the candidate biomarkers of challenge to 2-DG revealed by metabolomic HILIC analyses ($n = 6$). Features are designated as MXXXTYYY with XXX being the monoisotopic mass and YYY the retention time of the ion. Associated FC and ANOVA p -values are provided in Table 3. Features typed in blue were detected in positive-ion mode and those appearing in green arose in negative polarity.

CONCLUSION

The analytical strategy described herein streamlined the delineation of 13 features (6 lipids and 7 metabolites) as biomarkers of acute exposure to 2-DG, thereby proving the adequacy of the proposed workflow for metabolomics. Lipidomic analyses unveiled that 2-DG mainly altered the metabolism of a ceramide, the moderate elevation of this pro-apoptotic lipid being accompanied by a dramatic increase of the concentration of the pro-mitogenic glucosylceramides, which might be interpreted as a cytoprotective mechanism to circumvent the cytotoxicity of the former. These outcomes are consistent with former reports. Besides, metabolomic analyses revealed a tremendous increase of galactosylglycerol as well as slight elevations of several phosphatidylethanolamine and phosphatidylcholine derivatives. The current study was performed on a single HRMS analyzer including any limitation coming along with it. In such conditions, no structural resolution of the composite fatty acids is available, supporting an annotation by sum composition, as defined by lipidomics harmonizing guidelines, thus failing to

1 reach a single tentative candidate in cases where several hits were retrieved from databases.
2
3 Nevertheless, this limitation is not believed to represent a severe hindrance to decipher the
4 biological relevance of the dysregulated features outlined in this manuscript since the functional
5 roles of the lipid classes reported herein are not yet established on an individual molecular basis
6 but rather rely on lipid species group (*i.e.* long-chain ceramides vs very-long chain ceramides).
7
8 More generally speaking, lipid identification is widely regarded as the most challenging step in
9 the lipidomic workflow owing to the molecular complexity of the lipidome. Accordingly,
10 hyphenated strategies are increasingly being implemented in traditional lipidomic pipelines to
11 increase the confidence of lipid identification such as tandem mass spectrometric analyses that
12 are very often required to distinguish structures among numerous isobaric species or ion
13 mobility-mass spectrometry.
14
15
16
17
18
19
20

21 **ACKNOWLEDGMENTS**

22 The authors are indebted to the French Agency for Food, Environmental and Occupational
23 Health and Society (ANSES) for having funded this study through the project BEMAM
24 (BioElectroMagnétisme et Analyse Métabolomique – n° EST-2014/2 RF/012). Metabolomic
25 analyses used the instrumental facilities of LABERCA (Nantes).
26
27
28
29

30 **SUPPORTING INFORMATION**

31 The following files are available free of charge at ACS website <http://pubs.acs.org>:
32
33

34 Figure S1. PCA plots obtained from endocellular lipidomics sequences from the whole set of
35 features. Figure S2. PCA plots obtained from endocellular lipidomics sequences using a filtered
36 data set (features having both fold-change > 2, p-value < 0.05 and CV QC < 30%). Figure S3.
37 PCA plots obtained from endocellular metabolomics sequences from the whole set of features.
38 Figure S4. PCA plots obtained from endocellular lipidomics sequences from filtered data set
39 (features having both fold-change > 2, p-value < 0.05 and CV QC < 30%). Table S1.
40 Comparison of extraction procedures involving several solvent systems (R-XCMS data
41 processing). Table S2. CV values of internal and external standards among QC samples in
42 lipidomic sequences. Table S3. CV values of internal and external standards among QC samples
43 in metabolomic sequences. Table S4. Tentative identification of metabolites dysregulated upon
44 2-DG treatment. Table S5. Theoretical LogP values of putative metabolites identified during
45 metabolomic sequences. Red-typed values are not consistent with the retention time of the
46 feature. Table S6. Summary of the data from the 8 features found significant in the comparisons
47 2-DG vs Sham-exposed sample groups (lipidomics). Table S7. Summary of the data from the 8
48
49
50
51
52
53
54
55
56
57
58
59
60

1 features found significant in the comparisons 2-DG vs Sham-exposed sample groups
2 (metabolomics).
3
4

5 References

- 6
7
8 (1) Vander Heiden, M. G.; Cantley, L. C.; Thompson, C. B. Understanding the Warburg Effect: The
9 Metabolic Requirements of Cell Proliferation. *Science* **2009**, *324* (5930), 1029–1033.
- 10 (2) Hanahan, D.; Weinberg, R. A. Hallmarks of cancer: the next generation. *Cell* **2011**, *144* (5), 646–
11 674.
- 12 (3) Liu, H.; Hu, Y. P.; Savaraj, N.; Priebe, W.; Lampidis, T. J. Hypersensitization of Tumor Cells to
13 Glycolytic Inhibitors[†]. *Biochemistry (Mosc.)* **2001**, *40* (18), 5542–5547.
- 14 (4) Liu, H.; Savaraj, N.; Priebe, W.; Lampidis, T. J. Hypoxia increases tumor cell sensitivity to glycolytic
15 inhibitors: a strategy for solid tumor therapy (Model C). *Biochem. Pharmacol.* **2002**, *64* (12),
16 1745–1751.
- 17 (5) Pelicano, H.; Martin, D. S.; Xu, R.-H.; Huang, P. Glycolysis inhibition for anticancer treatment.
18 *Oncogene* **2006**, *25* (34), 4633–4646.
- 19 (6) Xu, R.; Pelicano, H.; Zhou, Y.; Carew, J. S.; Feng, L.; Bhalla, K. N.; Keating, M. J.; Huang, P.
20 Inhibition of glycolysis in cancer cells: a novel strategy to overcome drug resistance associated
21 with mitochondrial respiratory defect and hypoxia. *Cancer Res.* **2005**, *65* (2), 613–621.
- 22 (7) Stein, M.; Lin, H.; Jeyamohan, C.; Dvorzhinski, D.; Gounder, M.; Bray, K.; Eddy, S.; Goodin, S.;
23 White, E.; DiPaola, R. S. Targeting tumor metabolism with 2-deoxyglucose in patients with
24 castrate-resistant prostate cancer and advanced malignancies. *The Prostate* **2010**, *70* (13), 1388–
25 1394.
- 26 (8) Singh, D.; Banerji, A. K.; Dwarakanath, B. S.; Tripathi, R. P.; Gupta, J. P.; Mathew, T. L.;
27 Ravindranath, T.; Jain, V. Optimizing Cancer Radiotherapy with 2-Deoxy-D-Glucose: Dose
28 Escalation Studies in Patients with Glioblastoma Multiforme. *Strahlenther. Onkol.* **2005**, *181* (8),
29 507–514.
- 30 (9) Mohanti, B. K.; Rath, G. K.; Anantha, N.; Kannan, V.; Das, B. S.; Chandramouli, B. A.; Banerjee, A.
31 K.; Das, S.; Jena, A.; Ravichandran, R.; et al. Improving cancer radiotherapy with 2-deoxy-D-
32 glucose: phase I/II clinical trials on human cerebral gliomas. *Int. J. Radiat. Oncol. Biol. Phys.* **1996**,
33 *35* (1), 103–111.
- 34 (10) Raez, L. E.; Papadopoulos, K.; Ricart, A. D.; Chiorean, E. G.; DiPaola, R. S.; Stein, M. N.; Rocha
35 Lima, C. M.; Schlesselman, J. J.; Tolba, K.; Langmuir, V. K.; et al. A phase I dose-escalation trial of
36 2-deoxy-d-glucose alone or combined with docetaxel in patients with advanced solid tumors.
37 *Cancer Chemother. Pharmacol.* **2013**, *71* (2), 523–530.
- 38 (11) Ralser, M.; Wamelink, M. M.; Struys, E. A.; Joppich, C.; Krobitch, S.; Jakobs, C.; Lehrach, H. A
39 catabolic block does not sufficiently explain how 2-deoxy-D-glucose inhibits cell growth. *Proc.*
40 *Natl. Acad. Sci.* **2008**, *105* (46), 17807–17811.
- 41 (12) O'Donnell, A. F.; McCartney, R. R.; Chandrashekarappa, D. G.; Zhang, B. B.; Thorner, J.; Schmidt,
42 M. C. 2-Deoxyglucose Impairs *Saccharomyces cerevisiae* Growth by Stimulating Snf1-Regulated
43 and α -Arrestin-Mediated Trafficking of Hexose Transporters 1 and 3. *Mol. Cell. Biol.* **2015**, *35* (6),
44 939–955.
- 45 (13) Kang, H. T.; Hwang, E. S. 2-Deoxyglucose: An anticancer and antiviral therapeutic, but not any
46 more a low glucose mimetic. *Life Sci.* **2006**, *78* (12), 1392–1399.
- 47 (14) McCartney, R. R.; Chandrashekarappa, D. G.; Zhang, B. B.; Schmidt, M. C. Genetic Analysis of
48 Resistance and Sensitivity to 2-Deoxyglucose in *Saccharomyces cerevisiae*. *Genetics* **2014**, *198* (2),
49 635–646.
- 50 (15) Jaspers, H. T. A.; Van Steveninck, J. Transport-associated phosphorylation of 2-deoxy-D-glucose in
51 *Saccharomyces fragilis*. *Biochim. Biophys. Acta BBA-Biomembr.* **1975**, *406* (3), 370–385.
- 52 (16) Loba, Z.; Maitra, P. K. Resistance to 2-deoxyglucose in yeast: a direct selection of mutants lacking
53 glucose-phosphorylating enzymes. *Mol. Gen. Genet. MGG* **1977**, *157* (3), 297–300.
- 54 (17) Farkaš, V.; Svoboda, A.; Bauer, Š. Secretion of cell-wall glycoproteins by yeast protoplasts. Effect
55 of 2-deoxy-D-glucose and cycloheximide. *Biochem. J.* **1970**, *118* (5), 755–758.
- 56
57
58
59
60

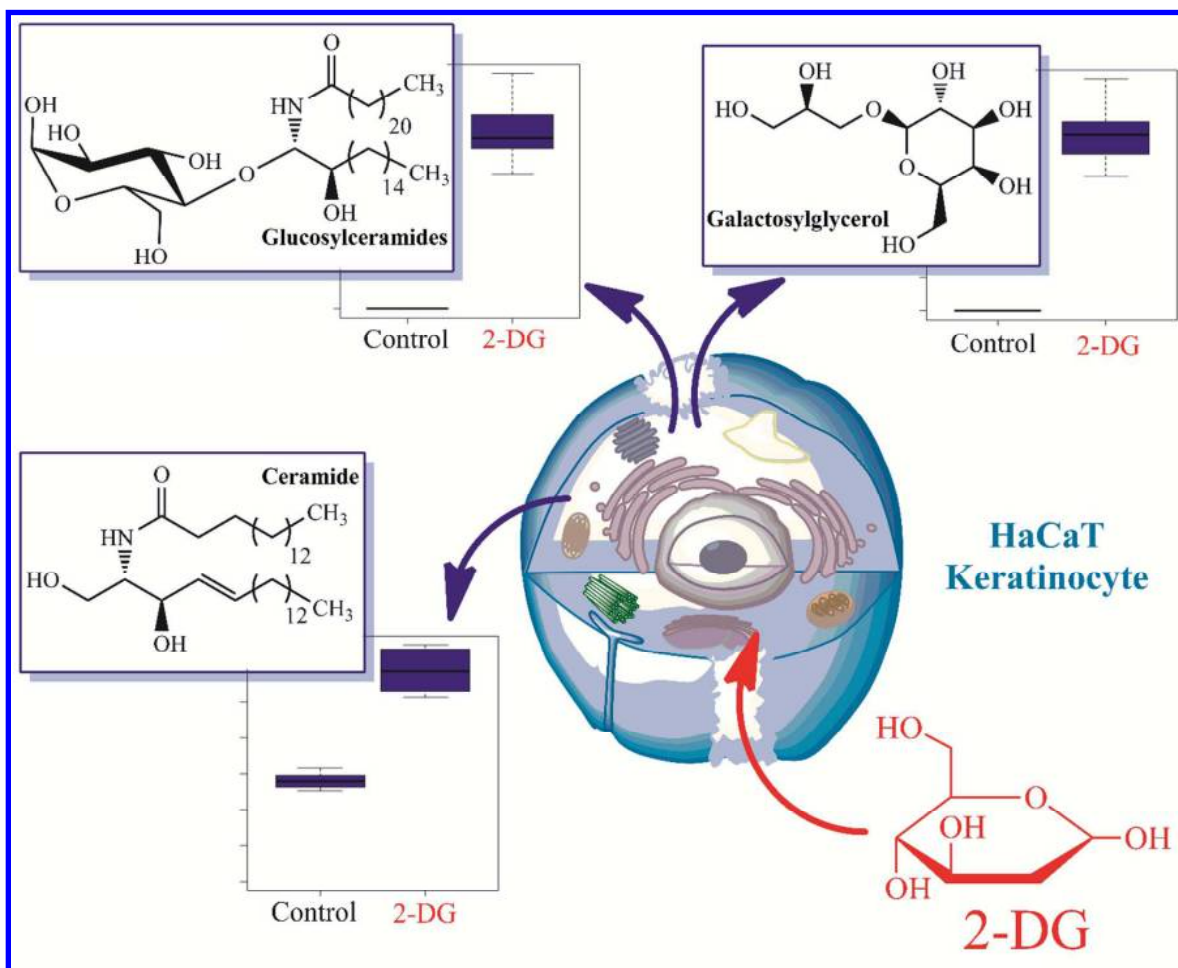
- 1
2
3
4
5
6
7
8
9
10
11
12
13
14
15
16
17
18
19
20
21
22
23
24
25
26
27
28
29
30
31
32
33
34
35
36
37
38
39
40
41
42
43
44
45
46
47
48
49
50
51
52
53
54
55
56
57
58
59
60
- (18) Kratky, Z.; Biely, P.; Bauer, Š. Mechanism of 2-Deoxy-d-glucose Inhibition of Cell-Wall Polysaccharide and Glycoprotein Biosyntheses in *Saccharomyces cerevisiae*. *Eur. J. Biochem.* **1975**, *54* (2), 459–467.
- (19) Datema, R.; Schwarz, R. T. Formation of 2-Deoxyglucose-Containing Lipid-Linked Oligosaccharides. *Eur. J. Biochem.* **1978**, *90* (3), 505–516.
- (20) Xi, H.; Kurtoglu, M.; Liu, H.; Wangpaichitr, M.; You, M.; Liu, X.; Savaraj, N.; Lampidis, T. J. 2-Deoxy-d-glucose activates autophagy via endoplasmic reticulum stress rather than ATP depletion. *Cancer Chemother. Pharmacol.* **2011**, *67* (4), 899–910.
- (21) Xi, H.; Barredo, J. C.; Merchan, J. R.; Lampidis, T. J. Endoplasmic reticulum stress induced by 2-deoxyglucose but not glucose starvation activates AMPK through CaMKK β leading to autophagy. *Biochem. Pharmacol.* **2013**, *85* (10), 1463–1477.
- (22) Ramirez-Peinado, S.; Alcazar-Limones, F.; Lagares-Tena, L.; El Mjiyad, N.; Caro-Maldonado, A.; Tirado, O. M.; Munoz-Pinedo, C. 2-Deoxyglucose Induces Noxa-Dependent Apoptosis in Alveolar Rhabdomyosarcoma. *Cancer Res.* **2011**, *71* (21), 6796–6806.
- (23) Soubere Mahamoud, Y.; Aite, M.; Martin, C.; Zhadobov, M.; Sauleau, R.; Le Dréan, Y.; Habauzit, D. Additive Effects of Millimeter Waves and 2-Deoxyglucose Co-Exposure on the Human Keratinocyte Transcriptome. *PLOS ONE* **2016**, *11* (8), e0160810.
- (24) Čuperlović-Culf, M.; Barnett, D. A.; Culf, A. S.; Chute, I. Cell culture metabolomics: applications and future directions. *Drug Discov. Today* **2010**, *15* (15), 610–621.
- (25) Ceglarek, U.; Shackleton, C.; Stanczyk, F. Z.; Adamski, J. Steroid profiling and analytics: going towards sterome. *J. Steroid Biochem. Mol. Biol.* **2010**, *121*, 479–480.
- (26) Wang-Sattler, R.; Yu, Y.; Mittelstrass, K.; Lattka, E.; Altmaier, E.; Gieger, C.; Ladwig, K. H.; Dahmen, N.; Weinberger, K. M.; Hao, P.; et al. Metabolic Profiling Reveals Distinct Variations Linked to Nicotine Consumption in Humans — First Results from the KORA Study. *PLoS ONE* **2008**, *3* (12), e3863.
- (27) Altmaier, E.; Kastenmüller, G.; Römisch-Margl, W.; Thorand, B.; Weinberger, K. M.; Adamski, J.; Illig, T.; Döring, A.; Suhre, K. Variation in the human lipidome associated with coffee consumption as revealed by quantitative targeted metabolomics. *Mol. Nutr. Food Res.* **2009**, *53* (11), 1357–1365.
- (28) Kell, D. B.; Goodacre, R. Metabolomics and systems pharmacology: why and how to model the human metabolic network for drug discovery. *Drug Discov. Today* **2014**, *19* (2), 171–182.
- (29) Sreekumar, A.; Poisson, L. M.; Rajendiran, T. M.; Khan, A. P.; Cao, Q.; Yu, J.; Laxman, B.; Mehra, R.; Lonigro, R. J.; Li, Y.; et al. Metabolomic profiles delineate potential role for sarcosine in prostate cancer progression. *Nature* **2009**, *457* (7231), 910–914.
- (30) Misek, D. E.; Kim, E. H. Protein Biomarkers for the Early Detection of Breast Cancer. *Int. J. Proteomics* **2011**, *2011*, 1–9.
- (31) Wang-Sattler, R.; Yu, Z.; Herder, C.; Messias, A. C.; Floegel, A.; He, Y.; Heim, K.; Campillos, M.; Holzappel, C.; Thorand, B.; et al. Novel biomarkers for pre-diabetes identified by metabolomics. *Mol. Syst. Biol.* **2012**, *8*, 615.
- (32) Hyötyläinen, T. Novel methodologies in metabolic profiling with a focus on molecular diagnostic applications. *Expert Rev. Mol. Diagn.* **2012**, *12* (5), 527–538.
- (33) Dunn, W. B.; Ellis, D. I. Metabolomics: Current analytical platforms and methodologies. *TrAC Trends Anal. Chem.* **2005**, *24* (4), 285–294.
- (34) Folch, J.; Lees, M.; Sloane Stanley, G. H. A simple method for the isolation and purification of total lipides from animal tissues. *J. Biol. Chem.* **1957**, *226*, 497–509.
- (35) Bligh, E. G.; Dyer, W. J. A rapid method of total lipid extraction and purification. *Can. J. Biochem. Physiol.* **1959**, *37* (8), 911–917.
- (36) Watson, A. D. Thematic review series: Systems Biology Approaches to Metabolic and Cardiovascular Disorders. Lipidomics: a global approach to lipid analysis in biological systems. *J. Lipid Res.* **2006**, *47* (10), 2101–2111.
- (37) Dettmer, K.; Nürnbergger, N.; Kaspar, H.; Gruber, M. A.; Almstetter, M. F.; Oefner, P. J. Metabolite extraction from adherently growing mammalian cells for metabolomics studies: optimization of harvesting and extraction protocols. *Anal. Bioanal. Chem.* **2011**, *399* (3), 1127–1139.

- 1
2
3
4
5
6
7
8
9
10
11
12
13
14
15
16
17
18
19
20
21
22
23
24
25
26
27
28
29
30
31
32
33
34
35
36
37
38
39
40
41
42
43
44
45
46
47
48
49
50
51
52
53
54
55
56
57
58
59
60
- (38) Matyash, V.; Liebisch, G.; Kurzchalia, T. V.; Shevchenko, A.; Schwudke, D. Lipid extraction by methyl-tert-butyl ether for high-throughput lipidomics. *J. Lipid Res.* **2008**, *49* (5), 1137–1146.
- (39) Xiao, J. F.; Zhou, B.; Resson, H. W. Metabolite identification and quantitation in LC-MS/MS-based metabolomics. *TrAC Trends Anal. Chem.* **2012**, *32*, 1–14.
- (40) Trygg, J.; Holmes, E.; Lundstedt, T. Chemometrics in metabonomics. *J. Proteome Res.* **2007**, *6* (2), 469–479.
- (41) Le Quément, C.; Nicolaz, C. N.; Habauzit, D.; Zhadobov, M.; Sauleau, R.; Le Dréan, Y. Impact of 60-GHz millimeter waves and corresponding heat effect on endoplasmic reticulum stress sensor gene expression: ER Stress Under MMW Exposure. *Bioelectromagnetics* **2014**, *35* (6), 444–451.
- (42) Halama, A. Metabolomics in cell culture—A strategy to study crucial metabolic pathways in cancer development and the response to treatment. *Arch. Biochem. Biophys.* **2014**, *564*, 100–109.
- (43) Kerdivel, G.; Boudot, A.; Habauzit, D.; Percevault, F.; Demay, F.; Pakdel, F.; Flouriot, G. Activation of the MKL1/actin signaling pathway induces hormonal escape in estrogen-responsive breast cancer cell lines. *Mol. Cell. Endocrinol.* **2014**, *390* (1–2), 34–44.
- (44) León, Z.; García-Cañaveras, J. C.; Donato, M. T.; Lahoz, A. Mammalian cell metabolomics: Experimental design and sample preparation. *Electrophoresis* **2013**, *34*, 2762–2775.
- (45) Batista, U.; Garvas, M.; Nemeč, M.; Schara, M.; Veranič, P.; Koklic, T. Effects of different detachment procedures on viability, nitroxide reduction kinetics and plasma membrane heterogeneity of V-79 cells. *Cell Biol. Int.* **2010**, *34* (6), 663–668.
- (46) Paglia, G.; Hrafnadóttir, S.; Magnúsdóttir, M.; Fleming, R. M. T.; Thorlacius, S.; Pálsson, B. Ø.; Thiele, I. Monitoring metabolites consumption and secretion in cultured cells using ultra-performance liquid chromatography quadrupole–time of flight mass spectrometry (UPLC–Q–ToF-MS). *Anal. Bioanal. Chem.* **2012**, *402* (3), 1183–1198.
- (47) Wehrens, R.; Hageman, J. A.; van Eeuwijk, F.; Kooke, R.; Flood, P. J.; Wijnker, E.; Keurentjes, J. J. B.; Lommen, A.; van Eekelen, H. D. L. M.; Hall, R. D.; et al. Improved batch correction in untargeted MS-based metabolomics. *Metabolomics* **2016**, *12* (5), 88.
- (48) Brunius, C.; Shi, L.; Landberg, R. Large-scale untargeted LC-MS metabolomics data correction using between-batch feature alignment and cluster-based within-batch signal intensity drift correction. *Metabolomics* **2016**, *12* (11), 173.
- (49) Chetwynd, A. J.; Abdul-Sada, A.; Holt, S. G.; Hill, E. M. Use of a pre-analysis osmolality normalisation method to correct for variable urine concentrations and for improved metabolomic analyses. *J. Chromatogr. A* **2016**, *1431*, 103–110.
- (50) Smith, C. A.; Want, E. J.; O’Maille, G.; Abagyan, R.; Siuzdak, G. XCMS: Processing Mass Spectrometry Data for Metabolite Profiling Using Nonlinear Peak Alignment, Matching, and Identification. *Anal. Chem.* **2006**, *78* (3), 779–787.
- (51) Smith, C. A.; O’Maille, G.; Want, E. J.; Qin, C.; Trauger, S. A.; Brandon, T. R.; Custodio, D. E.; Abagyan, R.; Siuzdak, G. METLIN: a metabolite mass spectral database. *Ther. Drug Monit.* **2005**, *27* (6), 747–751.
- (52) Tautenhahn, R.; Patti, G. J.; Rinehart, D.; Siuzdak, G. XCMS Online: A Web-Based Platform to Process Untargeted Metabolomic Data. *Anal. Chem.* **2012**, *84* (11), 5035–5039.
- (53) Wishart, D. S.; Tzur, D.; Knox, C.; Eisner, R.; Guo, A. C.; Young, N.; Cheng, D.; Jewell, K.; Arndt, D.; Sawhney, S.; et al. HMDB: the Human Metabolome Database. *Nucleic Acids Res.* **2007**, *35* (Database), D521–D526.
- (54) Wishart, D. S.; Jewison, T.; Guo, A. C.; Wilson, M.; Knox, C.; Liu, Y.; Djoumbou, Y.; Mandal, R.; Aziat, F.; Dong, E.; et al. HMDB 3.0—The Human Metabolome Database in 2013. *Nucleic Acids Res.* **2013**, *41* (D1), D801–D807.
- (55) Fahy, E.; Subramaniam, S.; Murphy, R. C.; Nishijima, M.; Raetz, C. R. H.; Shimizu, T.; Spener, F.; van Meer, G.; Wakelam, M. J. O.; Dennis, E. A. Update of the LIPID MAPS comprehensive classification system for lipids. *J. Lipid Res.* **2008**, *50* (Supplement), S9–S14.
- (56) Nicolas Nicolaz, C.; Zhadobov, M.; Desmots, F.; Sauleau, R.; Thouroude, D.; Michel, D.; Le Drean, Y. Absence of direct effect of low-power millimeter-wave radiation at 60.4 GHz on endoplasmic reticulum stress. *Cell Biol. Toxicol.* **2009**, *25* (5), 471–478.

- 1
2 (57) Ikeda, J.; Kaneda, S.; Kuwabara, K.; Ogawa, S.; Kobayashi, T.; Matsumoto, M.; Yura, T.; Yanagi, H.
3 Cloning and expression of cDNA encoding the human 150 kDa oxygen-regulated protein, ORP150.
4 *Biochem. Biophys. Res.* **1997**, *230* (1), 94–99.
- 5 (58) Zhang, H.; Lu, M.; Qi, H. B.; Zhang, J. H. Up-regulation of glucose regulated protein 78 induced by
6 2-deoxy-glucose plays a protective role for fetal rat cerebral neuron following intrauterine
7 distress. *Zhonghua Fu Chan Ke Za Zhi* **2008**, *43*, 356–360.
- 8 (59) Nagano, K.; Kano, H.; Arito, H.; Yamamoto, S.; Matsushima, T. Enhancement of Renal
9 Carcinogenicity by Combined Inhalation and Oral Exposures to Chloroform in Male Rats. *J.*
10 *Toxicol. Environ. Health A* **2006**, *69* (20), 1827–1842.
- 11 (60) Schmid, P.; Hunter, E.; Calvert, J. Extraction and purification of lipids. III. Serious limitations of
12 chloroform and chloroform-methanol in lipid investigations. *Physiol. Chem. Phys. Med. NMR*
13 **1973**, *5*, 151–155.
- 14 (61) Li, L.; Lu, X.; Zhao, J.; Zhang, J.; Zhao, Y.; Zhao, C.; Xu, G. Lipidome and metabolome analysis of
15 fresh tobacco leaves in different geographical regions using liquid chromatography–mass
16 spectrometry. *Anal. Bioanal. Chem.* **2015**, *407* (17), 5009–5020.
- 17 (62) Li, L.; Zhao, J.; Zhao, Y.; Lu, X.; Zhou, Z.; Zhao, C.; Xu, G. Comprehensive investigation of tobacco
18 leaves during natural early senescence via multi-platform metabolomics analyses. *Sci. Rep.* **2016**,
19 *6* (1), 37976.
- 20 (63) Cajka, T.; Fiehn, O. Toward Merging Untargeted and Targeted Methods in Mass Spectrometry-
21 Based Metabolomics and Lipidomics. *Anal. Chem.* **2016**, *88* (1), 524–545.
- 22 (64) Kouassi Nzoughe, J.; Bocca, C.; Simard, G.; Prunier-Mirebeau, D.; Chao de la Barca, J. M.;
23 Bonneau, D.; Procaccio, V.; Prunier, F.; Lenaers, G.; Reynier, P. A Nontargeted UHPLC-HRMS
24 Metabolomics Pipeline for Metabolite Identification: Application to Cardiac Remote Ischemic
25 Preconditioning. *Anal. Chem.* **2017**, *89* (3), 2138–2146.
- 26 (65) Want, E. J.; Wilson, I. D.; Gika, H.; Theodoridis, G.; Plumb, R. S.; Shockcor, J.; Holmes, E.;
27 Nicholson, J. K. Global metabolic profiling procedures for urine using UPLC-MS. *Nat. Protoc.* **2010**,
28 *5*, 1005–1018.
- 29 (66) Kim, N.; Ryu, S. M.; Lee, D.; Lee, J. W.; Seo, E.-K.; Lee, J.-H.; Lee, D. A metabolomic approach to
30 determine the geographical origins of *Anemarrhena asphodeloides* by using UPLC–QTOF MS. *J.*
31 *Pharm. Biomed. Anal.* **2014**, *92*, 47–52.
- 32 (67) Grösch, S.; Schiffmann, S.; Geisslinger, G. Chain length-specific properties of ceramides. *Prog.*
33 *Lipid Res.* **2012**, *51* (1), 50–62.
- 34 (68) Pettus, B. J.; Chalfant, C. E.; Hannun, Y. A. Ceramide in apoptosis: an overview and current
35 perspectives. *Biochim. Biophys. Acta BBA-Mol. Cell Biol. Lipids* **2002**, *1585* (2), 114–125.
- 36 (69) Siskind, L. J.; Kolesnick, R. N.; Colombini, M. Ceramide Channels Increase the Permeability of the
37 Mitochondrial Outer Membrane to Small Proteins. *J. Biol. Chem.* **2002**, *277* (30), 26796–26803.
- 38 (70) Uchida, Y. Ceramide signaling in mammalian epidermis. *Biochim. Biophys. Acta BBA - Mol. Cell*
39 *Biol. Lipids* **2014**, *1841* (3), 453–462.
- 40 (71) Bleicher, R. J.; Cabot, M. C. Glucosylceramide synthase and apoptosis. *Biochim. Biophys. Acta*
41 *BBA-Mol. Cell Biol. Lipids* **2002**, *1585* (2), 172–178.
- 42 (72) Datta, S. C.; Radin, N. S. Stimulation of liver growth and DNA synthesis by glucosylceramide. *Lipids*
43 **1988**, *23* (5), 508–510.
- 44 (73) Shayman, J. A.; Deshmukh, G. D.; Mahdiyoun, S.; Thomas, T. P.; Wu, D.; Barcelon, F. S.; Radin, N.
45 S. Modulation of renal epithelial cell growth by glucosylceramide. Association with protein
46 kinase C, sphingosine, and diacylglycerol. *J. Biol. Chem.* **1991**, *266*, 22968–22974.
- 47 (74) Marchell, N. L.; Uchida, Y.; Brown, B. E.; Elias, P. M.; Holleran, W. M. Glucosylceramides Stimulate
48 Mitogenesis in Aged Murine Epidermis. *J. Invest. Dermatol.* **1998**, *110* (4), 383–387.
- 49 (75) Lavie, Y.; Cao, H.; Bursten, S. L.; Giuliano, A. E.; Cabot, M. C. Accumulation of glucosylceramides in
50 multidrug-resistant cancer cells. *J. Biol. Chem.* **1996**, *271* (32), 19530–19536.
- 51 (76) Gutiérrez-Iglesias, G.; Hurtado, Y.; Palma-Lara, I.; López-Marure, R. Resistance to the
52 antiproliferative effect induced by a short-chain ceramide is associated with an increase of
53 glucosylceramide synthase, P-glycoprotein, and multidrug-resistance gene-1 in cervical cancer
54 cells. *Cancer Chemother. Pharmacol.* **2014**, *74* (4), 809–817.
- 55
56
57
58
59
60

- 1
2
3
4
5
6
7
8
9
10
11
12
13
14
15
16
17
18
19
20
21
22
23
24
25
26
27
28
29
30
31
32
33
34
35
36
37
38
39
40
41
42
43
44
45
46
47
48
49
50
51
52
53
54
55
56
57
58
59
60
- (77) Uchida, Y.; Murata, S.; Schmuth, M.; Behne, M. J.; Lee, J. D.; Ichikawa, S.; Elias, P. M.; Hirabayashi, Y.; Holleran, W. M. Glucosylceramide synthesis and synthase expression protect against ceramide-induced stress. *J. Lipid Res.* **2002**, *43* (8), 1293–1302.
- (78) Bowden, J. A.; Heckert, A.; Ulmer, C. Z.; Jones, C. M.; Koelmel, J. P.; Abdullah, L.; Ahonen, L.; Alnouti, Y.; Armando, A.; Asara, J. M.; et al. Harmonizing Lipidomics: NIST Interlaboratory Comparison Exercise for Lipidomics using Standard Reference Material 1950 Metabolites in Frozen Human Plasma. *J. Lipid Res.* **2017**, *in press*, doi:jlrm079012.
- (79) Messner, M. C.; Cabot, M. C. Glucosylceramides in human. In *Sphingolipids as signaling and regulatory molecules*; Chalfant, C., Del Poeta, M., Eds.; Advances in experimental medicine and biology; Springer Science+Business Media ; Landes Bioscience: New York, N.Y. : Austin, Tex, 2010; pp 156–164.
- (80) Kavaliauskiene, S.; Skotland, T.; Sylvänne, T.; Simolin, H.; Klokk, T. I.; Torgersen, M. L.; Lingelem, A. B. D.; Simm, R.; Ekroos, K.; Sandvig, K. Novel actions of 2-deoxy-D-glucose: protection against Shiga toxins and changes in cellular lipids. *Biochem. J.* **2015**, No. 470, 23–37.
- (81) Liebisch, G.; Vizcaíno, J. A.; Köfeler, H.; Trötz Müller, M.; Griffiths, W. J.; Schmitz, G.; Spener, F.; Wakelam, M. J. Shorthand notation for lipid structures derived from mass spectrometry. *J. Lipid Res.* **2013**, *54*, 1523–1530.
- (82) Garate, J.; Fernández, R.; Lage, S.; Bestard-Escalas, J.; Lopez, D. H.; Reigada, R.; Khorrami, S.; Ginard, D.; Reyes, J.; Amengual, I.; et al. Imaging mass spectrometry increased resolution using 2-mercaptobenzothiazole and 2,5-diaminonaphthalene matrices: application to lipid distribution in human colon. *Anal. Bioanal. Chem.* **2015**, *407* (16), 4697–4708.
- (83) Hamilton, J. S.; Aguilar, R.; Petros, R. A.; Verbeck, G. F. DAPNe with micro-capillary separatory chemistry-coupled to MALDI-MS for the analysis of polar and non-polar lipid metabolism in one cell. *J. Am. Soc. Mass Spectrom.* **2017**, *28* (5), 918–928.
- (84) Perttu, E. K.; Kohli, A. G.; Szoka, F. C. Inverse-Phosphocholine Lipids: A Remix of a Common Phospholipid. *J. Am. Chem. Soc.* **2012**, *134* (10), 4485–4488.
- (85) Jackson, S. N.; Wang, H.-Y. J.; Woods, A. S. In situ structural characterization of phosphatidylcholines in brain tissue using MALDI-MS/MS. *J. Am. Soc. Mass Spectrom.* **2005**, *16* (12), 2052–2056.
- (86) Gaudin, M.; Panchal, M.; Auzeil, N.; Duyckaerts, C.; Brunelle, A.; Laprévote, O.; Touboul, D. Choline-containing phospholipids in microdissected human Alzheimer’s disease brain senile plaque versus neuropil. *Bioanalysis* **2012**, *4* (17), 2153–2159.
- (87) Stanley, E. G.; Jenkins, B. J.; Walker, C. G.; Koulman, A.; Browning, L.; West, A. L.; Calder, P. C.; Jebb, S. A.; Griffin, J. L. Lipidomics Profiling of Human Adipose Tissue Identifies a Pattern of Lipids Associated with Fish Oil Supplementation. *J. Proteome Res.* **2017**, *16* (9), 3168–3179.
- (88) Li, Z.; Vance, D. E. *Thematic Review Series: Glycerolipids*. Phosphatidylcholine and choline homeostasis. *J. Lipid Res.* **2008**, *49* (6), 1187–1194.

For TOC only



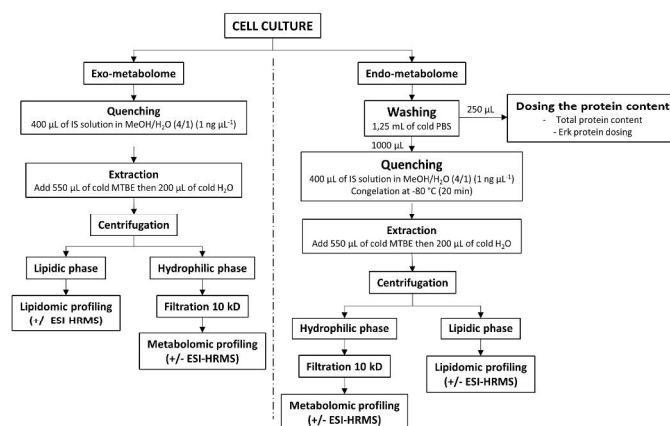


Figure 1 Schematic workflow of the analytical process for sample preparation.

355x266mm (300 x 300 DPI)

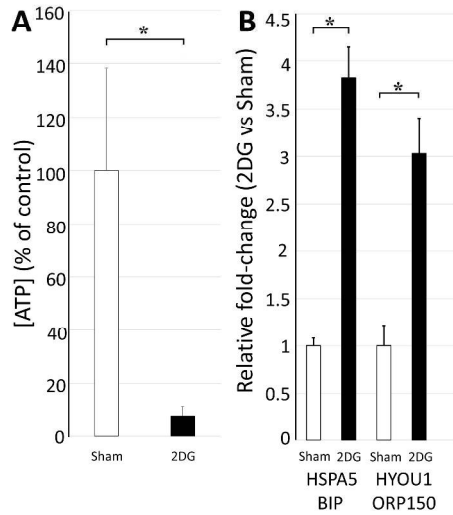


Figure 2 Comparison of intracellular ATP content (A) and mRNA levels of ER-resident chaperons involved in ER stress response (HSPA5/BIP and HYOU1/ORP150) (n = 3) (B) upon 2-DG treatment. *P < 0.01, Welch two-sample t test.

1562x1562mm (96 x 96 DPI)

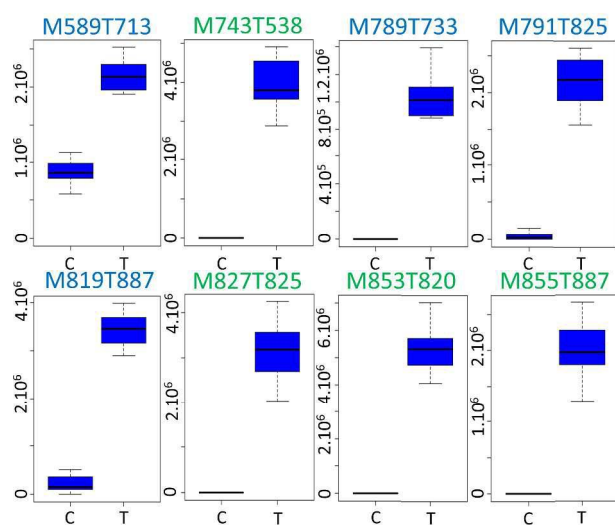


Figure 3 Box and whisker plots of the candidate biomarkers of treatment by 2-DG highlighted by lipidomic RPLC-MS analyses ($n = 6$). The y axis displays the normalized intensity of each metabolite. Features are designated as MXXXYYYY with XXX being the monoisotopic mass and YYY the retention time of the ion. Associated FC and ANOVA p-values are provided in Table 2. Features typed in blue were detected in positive-ion mode and those appearing in green arose in negative polarity.

340x536mm (300 x 300 DPI)

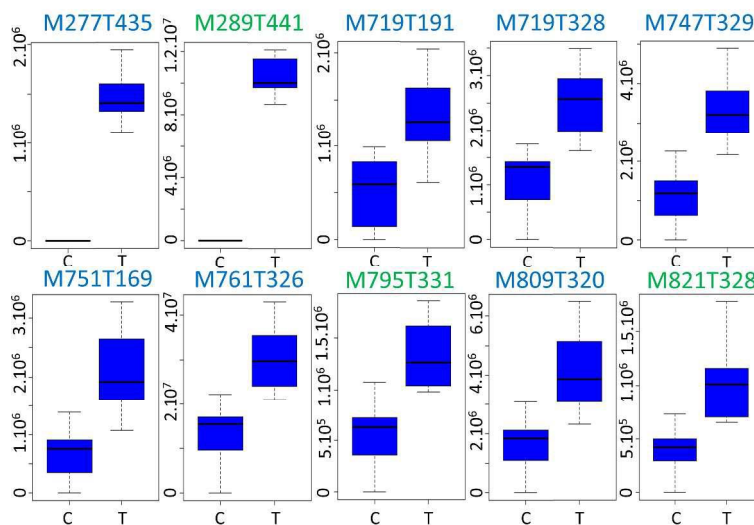


Figure 4 Box and whisker plots of the candidate biomarkers of challenge to 2-DG revealed by metabolomic HILIC analyses ($n = 6$). Features are designated as MXXXXTYYY with XXX being the monoisotopic mass and YYY the retention time of the ion. Associated FC and ANOVA p-values are provided in Table 3. Features typed in blue were detected in positive-ion mode and those appearing in green arose in negative polarity.

340x536mm (300 x 300 DPI)